Assessment of Demand Response Particibility Potential Based on Cost-Effective Process Design

Yu Liu, * **Gustavo Campos,** * **Ahmet Palazoglu,** *
Nael H. El-Farra *

* *University of California Davis, Davis, CA, 95616, USA (e-mail: nhelfarra@ucdavis.edu).*

Abstract: In this work, a model-based analytical framework is proposed to evaluate the cost-effectiveness of process design alternatives with respect to their ability to participate (particibility) in Demand Response (DR) services (such as load shifting under the Day-Ahead market) through the use of supply curves. The supply curves relate available DR capability to the investment cost of process design, and are constructed based on a specific DR service. Using the California Independent System Operator (CAISO) wholesale electricity market as a reference, the proposed framework is implemented to demonstrate the cost-benefits of considering DR aspects at the design stage. As a motivating example, the developed framework is illustrated using a CSTR-storage model, for which supply curves are generated under different scenarios. A visualization is provided of the effect of the process design capacities on the DR capability, as well as the limitations on the load-shifting capacity of a given process design.

Keywords: Demand Response, Process Design, Process Scheduling, Process Control, Supply Curves.

1. INTRODUCTION

Demand response (DR) has become increasingly important as a strategy for balancing the power supply and demand under an ambitious renewable portfolio standard, keeping the electric grid stable and efficient; deferring upgrades to generation, transmission and distribution systems; and providing other economic benefits to customers. Energy-intensive industries could participate in the electricity market through different DR mechanisms, providing stability to the grid system as well as lowering the operating costs (Gerke et al. (2020)). Generally, it is well-recognized that participation in the DR market requires that the specific energy-intensive process have sufficient operational flexibility, and that the process dynamics should also be fast enough to respond to the rapidly changing electricity price trends. One of the current bottlenecks for residential and commercial applications in terms of their ability to participate in the DR market is the lack of advanced control equipment; yet for large-end industrial electricity users, the cost of advanced metering to facilitate DR participation does not appear to be a significant barrier (Baldea (2017)); rather, DR design is an extremely important consideration when decisions for investments are made.

Currently, research in the DR area focuses mostly on the scheduling and operation of energy-intensive processes under time-varying electricity markets. In particular, the operation of a process with direct participation in the short-term market (e.g., Five-Minute Ahead Market) has

gained significant attention among researchers (see, for example, Dowling et al. (2017); Otashu and Baldea (2020)). Also, model-based bidding strategies for industrial processes have been investigated (e.g., see Schäfer et al. (2018)). Above works have investigated the participation of a fixed plant into the time-varying electricity market, but the flexibility potential on the demand side from the design perspective are not addressed. As for the design problem, Liu et al. (2020) studied the flexible design of a pump network under DR objectives, and Teichgraeber and Brandt (2020) explored the design of a chlor-alkali plant under the real-time electricity market (RTM). Both works used a stochastic programming framework to address the design problem; however, none of the current studies directly addressed the impact of process design or process dynamics (and the associated costs) on the ability of the process to participate in DR services. Incorporating DR objectives directly into the design and operation of chemical processes needs to take account of the plant capacity design as well as the intrinsic process dynamics, which usually introduces significant nonlinearities into the modeling. Furthermore, the design stage is usually at a different time scale compared to the DR operational decisions, which in general is in hours or even minutes, and thus a multi-scale model is usually required, often leading to an intractable model, where the impact of design on the DR capability is difficult to quantify.

Motivated by above considerations, the objective of this work is to systematically study the "cost-effectiveness" for the design of a process when considering the participation in the DR market (particibility), specifically, the Day-Ahead market (DAM). We propose a bottom-up approach,

starting with a first-principles dynamic model to construct a high fidelity process operating range and then implement the scheduling model to analyze a metric defined as "load-shifting capacity", which aims to quantify the DR capability under a specific DAM electricity price profile. The analysis is carried out under different design scenarios to provide the supply curve, which helps to demonstrate the relationship between investment and DR capability.

2. METHODOLOGY & MODEL FORMULATION

2.1 Problem Description

In this work, we present a bottom-up approach to analyze the relation between process design (in our case, the capital cost of the system) and load shifting potential, through the supply curves. The supply curve, which is widely used in the area of economics, is a graphical representation of the correlation between the cost of a good or service and the quantity supplied for a given period. In the sections that follow, we discuss the framework implemented in this work to analyze the cost-effectiveness of a certain process design. We define a new metric, namely *load-shifting capacity*, to quantify the DR capability of a given process in terms of load shifting. The *load-shifting capacity* metric is calculated using a scheduling-based model integrated with process dynamics.

2.2 Overview of Analysis Framework

The first step in the framework is to generate the feasible region for the operation-related decision variables. This is performed using a first-principles dynamic model for the given process. The specific focus of this part is to provide the scheduling model with a feasible operating range as well as the transition profile information. The feasible region not only includes the operating range but also provides information on whether specific operating adjustments will violate the system constraints such as safety concerns or production requirements. The second step is to develop a scheduling-oriented operating model to evaluate the potential of the load shifting under specific process design or capacity. Here, we define a new metric, shifted load, to quantify the DR capability. It is noted that this metric is used to evaluate the load-shifting capacity only under the DAM. As shown in Figure 1, the blue solid line represents the scheduled operating profile, while the orange dashed line represents the base load. Theoretically, if the total product demand remains unchanged over a period of time, the total production over time should not change. Therefore, the area under the blue line and the area under the orange line should be nearly equal for a given period of time. We define the base load at time t as E_t^b and the real scheduled load as E_t^s; thus we can quantify the *load-shifting capacity* as follows:

$$E^{shift} = \sum_t \frac{|E_t^b - E_t^s|}{2}. \tag{1}$$

As one might notice, this value is equal to the grey area in Figure 1. The last step in the proposed framework is to construct the supply curve to demonstrate the "cost-effectiveness" of various design alternatives. The scheduling model under different design parameters, such as reac-
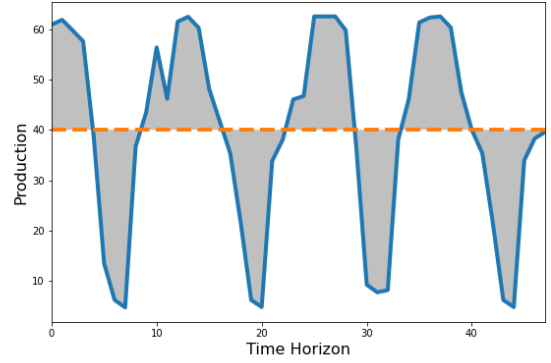
Fig. 1. Demonstration of the *load-shifting capacity* concept, where the blue line shows the real scheduled production, and the orange dashed line shows the base line.

tor size or inventory capacity, is implemented repeatedly, and the results are used to construct the supply curve.

Scheduling Model The scheduling model presented herein extends the model proposed in Tong et al. (2017). The objective function for the operation is defined as follows:

$$J_{schedule} = \min(\Phi_1 + \Phi_2 + \Phi_3), \tag{2}$$

where $\Phi_1 = \gamma \sum^T (P_t \pi_t)$, $\Phi_2 = \sum^T \delta^{raw} F_t$ and $\Phi_3 = \sum^T \delta^s S_t$. The terms Φ_1, Φ_2, and Φ_3 represent the energy cost, the raw materials cost, and the inventory cost, respectively. The parameter γ is the scaling factor that links the production to the electricity consumption. The terms P_t, F_t, and S_t represent the production rate at time t, the set-point for the production rate at time t, and the storage capacity at time t, respectively. π_t, δ^{raw} and δ^s represent the electricity price at time t, the raw material cost and the inventory cost, respectively.

Production and transition The production and transition model are provided as:

$$P_t = F_t(1 - t_t^{trans}), \tag{3}$$

where the production rate at time t, P_t, is set to the production rate set-point, F_t, times the production duration time, $1 - t_t^{trans}$, which implies that production over the transition time is treated as an off-spec product and is not counted towards production that satisfies the demand. The transition time is defined as:

$$t_t^{trans} = f(\mathbf{x_t}, \mathbf{\Delta x_t}). \tag{4}$$

The transition time t_t^{trans} here is defined as a function of the state variable $\mathbf{x_t}$, at time t, and the step change $\mathbf{\Delta x_t}$. It should be noted that in Tong et al. (2015), scheduling was considered between a discrete set of operating modes which were defined a priori. As a result, the transition time variables were treated as parameters. However, as the aim of the current scheduling formulation is to determine the optimal operating mode at any given time, a discretization strategy will not be practical here as the range of possible operating modes could be considered infinite. This will result in a significant increase in the number of binary variables in the original model, thus making it intractable.
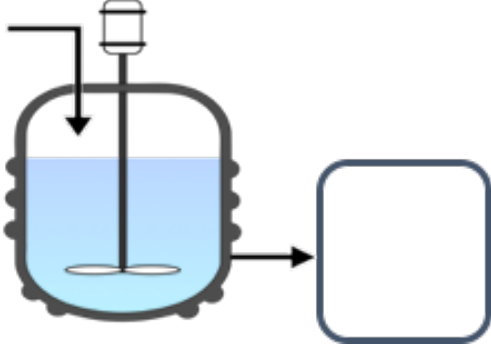
Fig. 2. A non-isothermal CSTR connected to a storage system.

In Beal et al. (2018), however, the transition time was estimated using the log function transformation. But it is worth pointing out that a linearized feedback control scheme was implemented in that study, and therefore provided a good fit only using the log function transformation.

The production rate set-point, F_t should also satisfy the bounds and ramping constraint given below:

$$F_t \in [F_{min}, F_{max}] \tag{5}$$
$$F_t - F_{t-1} \leq \delta, \tag{6}$$

where F_{min} and F_{max} define the minimum and maximum production set-points, and δ defines the ramping limit.

Inventory constraint   The inventory constraint are expressed as follows:

$$S_t = S_{t-1} + P_t - D_t, \tag{7}$$

where D_t is the demand at time step t. The bounds of the inventory are given as $0 \leq S_t \leq S_{max}$. Satisfying the hourly demand is a hard constraint, and thus the inventory tank is initially charged with a certain amount of on-spec product S_0, which will be defined as $S_0 = aS_{max}$, and a and is the percentage of the inventory size so as to make the DR problem feasible. Also, to avoid depleting the product, the storage at the end of the time period is set equal to the initial storage (periodic terminal constraint): $S_T \geq S_0$. It is important to note that the complexity of the above problem will depend on the transition time profile Eqn. [4], which could be treated as a fixed parameter or as a function. As a natural extension of the formulation in Tong et al. (2017), we replace the fixed parameter assumption and propose the use of a surrogate model for the transition time.

Definition of the capital cost   The capital cost is calculated as $log_{10}C = K_1 + K_2 log_{10}(A) + K_3[log_{10}(A)]^2$, where C is the capital investment; A is the capacity or size parameter for the equipment; and K_1, K_2, K_3 are the cost coefficients. The equation and the values of the parameters are taken from (Turton et al. (2018)).

3. CASE STUDY

We consider an illustrative case study inspired by earlier works (Tong et al. (2015); Beal et al. (2018)), where a non-isothermal CSTR is connected to a storage system as shown in Figure 2. While the CSTR is usually not considered as an electricity-intensive process, the nonlinear

dynamics of the system help to illustrate the proposed framework and analysis approach.

3.1 Dynamic process model

The dynamics of the non-isothermal CSTR are derived from standard material and energy balances and are captured by the following non-dimensionalized model:

$$\frac{dc}{dt} = \frac{1 - c(t)}{\theta} - k_0 e^{-\frac{n}{T}} c(t), \tag{8}$$
$$\frac{dT}{dt} = \frac{y_f - T(t)}{\theta} - k_0 e^{-\frac{n}{T}} c(t) + \alpha * u(t) * (y_c - T(t)), \tag{9}$$

where $\theta = \frac{V}{F}$, $\alpha = \frac{UA_c}{\rho C_p V}$, $y_f = \frac{\rho C_p T_f}{\Delta H}$, $n = \frac{E\rho C_p}{R\Delta H}$, $y_c = \frac{\rho C_p T_c}{\Delta H}$ and the state variables are $c = \frac{c_R}{c_f}$, and $T = \frac{\rho C_p T_R}{\Delta H}$. Meanwhile, the dimensionless temperature, T, needs to satisfy the constraint:

$$0 \leq T(t) \leq 1, \ \forall t. \tag{10}$$

In this study, the cooling water flowrate $u(t)$ is used as the only manipulated variable to control the reactor temperature. The above CSTR model, together with the process parameters, are taken from (Flores-Tlacuahuac et al. (2008)).

As mentioned earlier, the specific control scheme for the system could be designed differently. For example, in the earlier works (Tong et al. (2015, 2017)), a PID control scheme was implemented to execute the transitions between the different operating modes. For such a scheme, however, the transition dynamics are dependent on the choice of the PID tuning parameters. Given this, and the fact that the aim of the current study is to assess the DR potential for different design capacities, using a PID controller in this case would require that the PID settings be adjusted each time the design capacity is varied to ensure that a meaningful comparison between the various design alternatives is made without the added influence of the controller tuning. To eliminate the dependence on controller settings, we use in this study a dynamic optimization-based control scheme that automatically accounts for the transition effects. An exploration of the influence of different control strategies on the potential of DR participation is the subject of other research work.

The objective function for the optimal control problem is given by:

$$obj = \Sigma_t[\alpha(c(t) - c_s)^2 + \beta(u(t) - u(t-1))^2], \tag{11}$$

where α and β are the penalty weights, c_s is the target concentration of the desirable product. The objective function penalizes changes in the control action, as well as concentration set-point errors. The above dynamic optimization problem is solved using Pyomo (Hart et al. (2012)) and using the differential-algebraic equation package (Nicholson et al. (2018)). A sample transition profile is shown in Figure 3, where the transition occurs from the steady-state with $\theta = 60$ hr to the steady state with $\theta = 30$ hr.

3.2 Transition time space generation

In order to generate data points for the transition time profiles, the transition between two steady states corre-
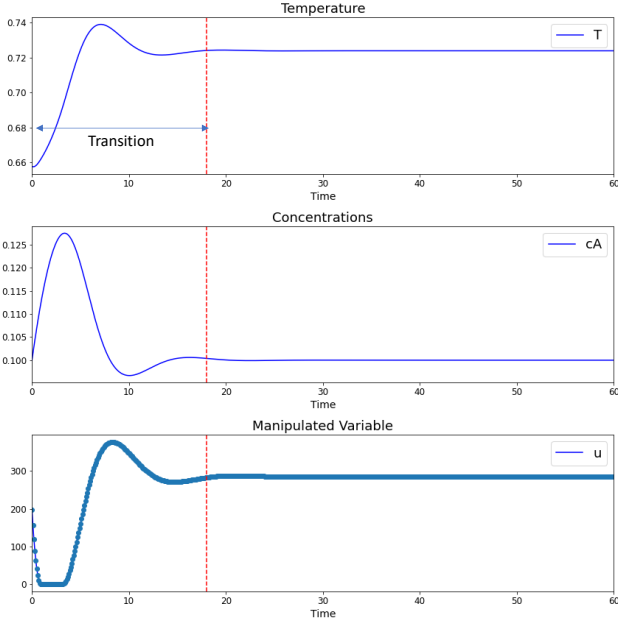
Fig. 3. CSTR state and input transition profiles from $\theta = 60$ to $\theta = 30$ hr.

sponding to different θ values, ranging from 8 to 80 hr, is simulated via dynamic optimization. The transition time value is then extracted from the profile obtained. Given that the time constant is defined as $\theta = \frac{V}{F}$, θ can be varied (for a given reactor volume V) by varying the inlet flowrate F. For different θ values, there will be different steady-states. Therefore, we vary θ to generate different steady-states, and, thereafter, simulate the transition profiles from one steady-state to another. As shown in (4), the state variable would be θ_t and the step change would be $\Delta\theta_t$ correspondingly. The relation between F_t in (3) and θ_t would be given as $F_t = \frac{V}{\theta_t}$. Also, F_{min} and F_{max} could be replaced by: $F_{min} = \frac{V}{\theta_{max}}$ and $F_{max} = \frac{V}{\theta_{min}}$.

All the simulations then provide a transition time space to be used subsequently in the scheduling model. Figure 4 shows an example transition time space visualization for a CSTR with a volume of 400 L. To incorporate this information into the scheduling model, as the constraint in (4), a functional relationship needs to be constructed. One way to construct a sample surrogate model is to utilize piecewise linear constraints. However, in general, this approach will significantly increase the size of the problem, since a significant number of binary variables is required to accurately represent the data. In this work, we formulate the transition time surface using the Big-M reformulation (Grossmann and Trespalacios (2013)).It worth to point out that in this work, an open-loop control of a non-linear dynamics system is implemented. This complicates the transition time space as shown in Figure 4. However, in real application, a closed-loop strategy might be implemented and thus, linearization of the system is possible.

3.3 Results

The scheduling problem with the Big-M transition time reformulation is solved in Pyomo with the Gurobi solver.
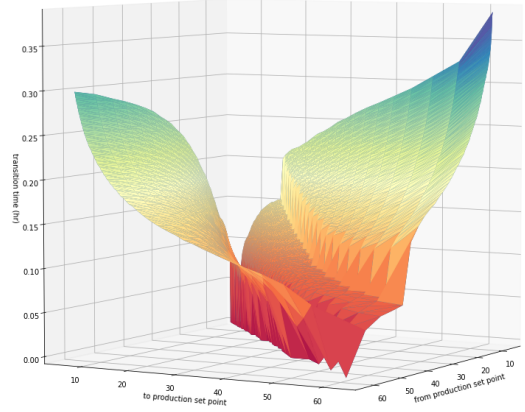
Fig. 4. Visualization of the transition time between two steady states (as a function of the starting and ending states) for a 400-L CSTR.
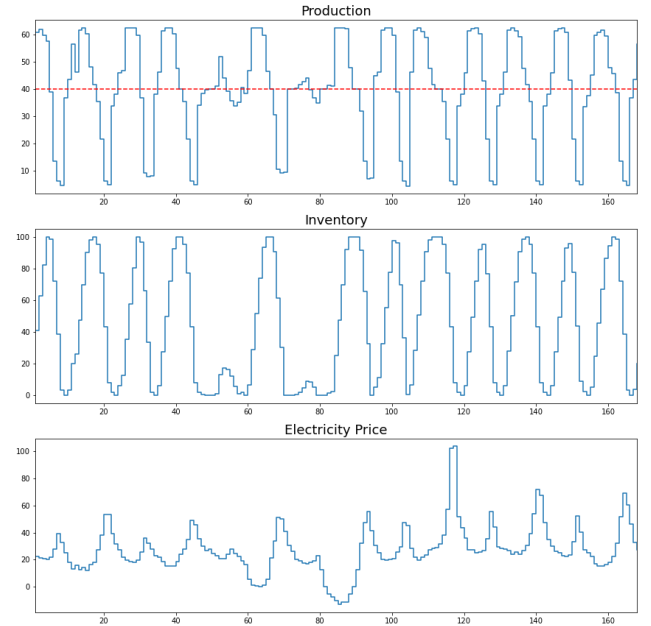
Fig. 5. Visualization of the operating profiles for a 400-L CSTR.

In Figure 5, a sample scheduling result for the production (top plot) and inventory (middle plot) under a representative electricity price profile (bottom plot) is shown. The representative electricity price is taken from an aggregated node in California for the first week in 2019. The inventory and production profiles under the provided representative electricity prices are met as expected, i.e., as the price increases the production rate decreases and vice versa. To construct the supply curve for a given case, a range of parameters are used in the dynamic and scheduling models. For the design specifications, the CSTR size and the storage capacity will be considered as the design variables.
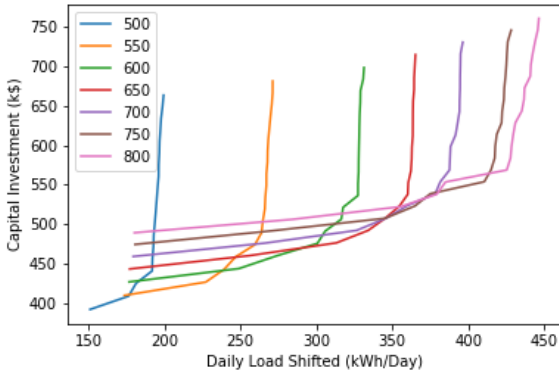
Fig. 6. Supply curves for different CSTR sizes.

Fig. 7. Supply curves for different storage sizes.

The CSTR size will range from 500 to 800 L, with an incremental increase of 50 L, while the storage size will range from 100 to 1000 L, with 50 L increments as well.

Supply curves under different CSTR sizes: Figure 6 shows the supply curves, where the capital cost is plotted as a function the daily shifted load, for different CSTR sizes (ranging from 500 to 800 L). The inventory cost parameter, δ^s, in this case is set to zero, while the hourly demand, D_t, is assumed to be constant and set to 50 L/hr. Therefore, for a given CSTR size, the cost in Figure 6 can be viewed as a function of the storage size as well.

The supply curve provides a visualization of the limitation of how much load a certain design choice could potentially shift for a given amount of capital investment. For example, for the CSTR size of 650 L, increasing the daily load-shifting capacity from 175 kWh to 350 kWh only requires a modest increase in capital investment; however, beyond 350 kWh the steep increase in the investment cost associated with the storage size suggests a limitation on the load-shifting capacity. It is intuitive to expect the range of daily load-shifting capacity to increase as the inventory size is increased. The supply curves, however, provide additional visual information regarding the limitation on the load-shifting capacity, implying that for a given CSTR design, while increasing the storage size could help increase the load-shifting capacity (and thus potentially yield profits from the DR load-shifting), there exists a limit beyond which the investment into additional storage capacity will no longer be cost-effective. As can be seen from the figure, this limit increases as the CSTR size increases, suggesting that larger CSTRs enjoy a wider range of "cost-effective" load-shifting capacities. Over this range, an increase in the load-shifting capacity requires only a modest increase in the storage investment cost.

Supply curves under different storage sizes: Figure 7 depicts the supply curves for different storage sizes, with the inventory cost, δ^s, set to zero and the hourly demand, D_t, set to 50 L/hr. In this case, for a given storage size, the cost in Figure 7 can be viewed as a function of the CSTR size as well. It can be seen that when the storage size is small, i.e., in the range from 100 to 300 L, the increase in the CSTR investment exhibits a trend similar to that in the supply curves in Figure 2, where an increase in the CSTR size helps expand the range of
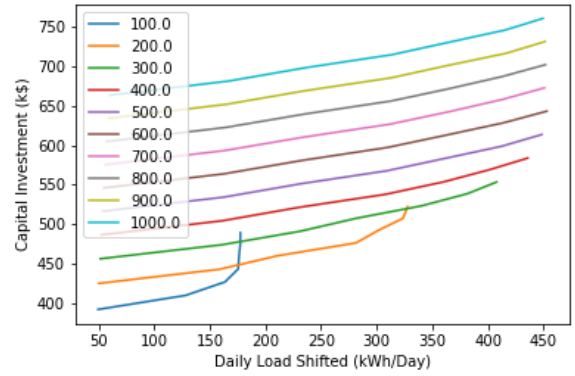
load-shifting capacities, but only up to a limit beyond which further CSTR size increases become no longer cost-effective. However, for larger storage sizes, i.e., in the range from 400 to 1000 L, the supply curves become parallel to one another, which suggests that after the storage reaches a certain size limit, to reach the same load-shifting capacity, an increase of the storage size does not provide any benefit. This is consistent with the trend observed earlier in Figure 6.

Supply curves under different inventory costs: So far in the analysis, we have assumed that no cost is associated with storing the product. To illustrate the limitations imposed by the cost of storing the product on the daily load-shifting capacity, we present in this part the supply curves for different values of the inventory cost parameter, δ_s. The supply curves for this scenario are presented in Figure 8. In this case, the hourly demand, D_t, is set to 50 L/hr and the CSTR size is set to 800 L. The results show that the daily load-shifting capacity is limited by the cost of storing the product. The case where $\delta^s = 0$ (i.e., no inventory cost) serves here as a base case. It can be seen that as the inventory cost increases, the supply curve shifts to the left, indicating a smaller range of cost-effective load-shifting capacities. The lower the inventory cost, the higher the capability of load shifting the system could reach. It is to be noted that when $\delta^s = 0$, the supply curve becomes almost vertical around a daily load-shifted value of 450 kWh/Day, which might also mean that the highest load-shifting for this system will be capped at around this value.

Supply curves under different hourly demands: In Figure 9, the supply curves for different values of the demand, D_t, are presented. In this case, the CSTR size is set to 800 L, while the inventory cost parameter δ^s is set to zero. It can be seen that as the demand increases, the cost-effective range of load-shifting capacities increases, and so does the limiting load-shifting capacity. It is also interesting that with the increase of the demand parameter, the distance between the supply curves decreases. For example, the supply curve for $D_t = 50$ L/hr almost overlaps with the supply curve for the case with $D_t = 60$. This suggests that given a fixed CSTR size the change in demand will no longer have an effect on the capability of load shifting.
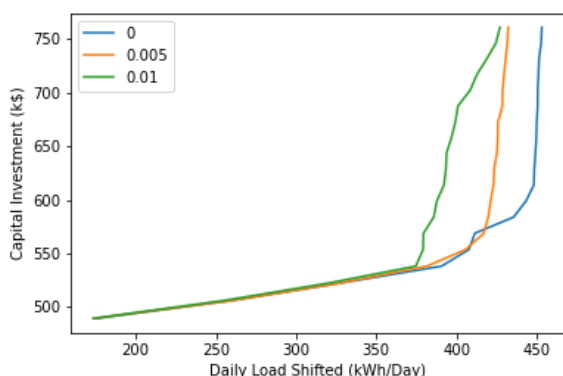
Fig. 8. Supply curves for different inventory costs, δ^s.
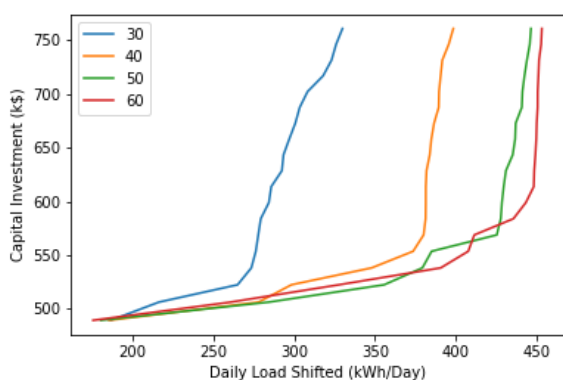
Fig. 9. Supply curves under different hourly demand values.

4. CONCLUSIONS

In this work, we presented a sequential model-based analytical framework for assessing the potential of a process to participate in DR load-shifting services based on the cost-effectiveness of various design alternatives. The framework brings together tools from dynamic modeling, optimal control and operational scheduling, and culminates in the construction of the system supply curves which quantify the link between the capital investment of a given design and its DR load-shifting capability. For a conceptual demonstration of the approach, a non-isothermal CSTR combined with a simple inventory system was considered as a case study. Future research work will focus on applying the proposed framework to a more complex and realistic case study, as well as directly incorporating the load shifting metric into the system design.

REFERENCES

Baldea, M. (2017). Employing Chemical Processes as Grid-Level Energy Storage Devices. In G.M. Kopanos, P. Liu, and M.C. Georgiadis (eds.), *Advances in Energy Systems Engineering*, 247—271. Springer International Publishing, Cham. doi:10.1007/978-3-319-42803-1_9. URL https://doi.org/10.1007/978-3-319-42803-1_9.

Beal, L.D., Petersen, D., Grimsman, D., Warnick, S., and Hedengren, J.D. (2018). Integrated Scheduling and Control in Discrete-time with Dynamic Parameters and Constraints. *Computers & Chemical Engineering*, 115, 361–376. doi:10.1016/j.compchemeng.2018.04.010.

Dowling, A.W., Kumar, R., and Zavala, V.M. (2017). A multi-scale optimization framework for electricity market participation. *Applied Energy*, 190, 147–164. doi:10.1016/j.apenergy.2016.12.081.

Flores-Tlacuahuac, A., Moreno, S.T., and Biegler, L.T. (2008). Global Optimization of Highly Nonlinear Dynamic Systems. *Industrial & Engineering Chemistry Research*, 47(8), 2643–2655. doi:10.1021/ie070379z.

Gerke, B.F., Gallo, G., Smith, S.J., Liu, J., Raghavan, S.V., Schwartz, P., Piette, M.A., Yin, R., and Stensson, S. (2020). The California Demand Response Potential Study, Phase 3: Final Report on the Shift Resource through 2030. Technical report.

Grossmann, I.E. and Trespalacios, F. (2013). Systematic modeling of discrete-continuous optimization models through generalized disjunctive programming. *AIChE Journal*, 59(9), 3276–3295. doi:10.1002/aic.14088.

Hart, W.E., Laird, C., Watson, J.P., and Woodruff, D.L. (2012). *Pyomo – Optimization Modeling in Python*. doi:10.1007/978-1-4614-3226-5_2.

Liu, Y., Fan, Y., Palazoglu, A., and El-Farra, N.H. (2020). A flexible design framework for process systems under demand-side management. *AIChE Journal*, 66(7). doi:10.1002/aic.16249.

Nicholson, B., Siirola, J.D., Watson, J.P., Zavala, V.M., and Biegler, L.T. (2018). pyomo.dae: a modeling and automatic discretization framework for optimization with differential and algebraic equations. *Mathematical Programming Computation*, 10(2), 187–223. doi:10.1007/s12532-017-0127-0.

Otashu, J.I. and Baldea, M. (2020). Scheduling chemical processes for frequency regulation. *Applied Energy*, 260, 114125. doi:10.1016/j.apenergy.2019.114125.

Schäfer, P., Westerholt, H.G., Schweidtmann, A.M., Ilieva, S., and Mitsos, A. (2018). Model-Based Bidding Strategies on the Primary Balancing Market for Energy-Intense Processes. *Computers & Chemical Engineering*, 120, 4–14. doi:10.1016/j.compchemeng.2018.09.026.

Teichgraeber, H. and Brandt, A.R. (2020). Optimal design of an electricity-intensive industrial facility subject to electricity price uncertainty: stochastic optimization and scenario reduction. *Chemical Engineering Research and Design*, 163, 204–216. doi:10.1016/j.cherd.2020.08.022.

Tong, C., Palazoglu, A., and El-Farra, N.H. (2017). A Decomposition Scheme for Integration of Production Scheduling and Control: Demand Response to Varying Electricity Prices. *Industrial & Engineering Chemistry Research*. doi:10.1021/acs.iecr.7b00869.

Tong, C., Palazoglu, A., El-Farra, N.H., and Yan, X. (2015). Energy demand management for process systems through production scheduling and control. *AIChE Journal*, 61(11), 3756–3769. doi:10.1002/aic.15033.

Turton, R., Shaeiwitz, J., Bhattacharyya, D., and Whiting, W. (2018). *Analysis, Synthesis, and Design of Chemical Processes: Analy Synth Desig Chemi Pr_5*. International Series in the Physical and Chemical Engineering Sciences. Pearson Education. URL https://books.google.com/books?id=eV5gDwAAQBAJ.